Available online at www.sciencedirect.com

SciVerse ScienceDirect

Ceramics International 39 (2013) 475–481

CERAMICS INTERNATIONAL

www.elsevier.com/locate/ceramint

Comparative study on effect of oxide thickness on stress distribution of traditional and nanostructured zirconia coating systems

Musharaf Abbas[a], Hongbo Guo[a,*], Muhammad Ramzan Shahid[b]

[a]Key Laboratory of Aerospace Materials and Performance (Ministry of Education), School of Materials Science and Engineering, Beihang University, No. 37 Xueyuan Road, Beijing 100191, China

[b]National University of Sciences and Technology, H-12, Islamabad 44000, Pakistan

Received 24 April 2012; received in revised form 17 June 2012; accepted 17 June 2012
Available online 23 June 2012

Abstract

Numerical based assessment of traditional and nanostructured yttria stabilized zirconia (YSZ) thermal barrier coating systems (TBCs) has been carried out with varying thickness of thermally grown oxide (TGO). Radial, axial and shear stresses are determined for both coatings and are presented in comparison with few novel and interesting results. Elastic strain energy for TGO failure assessment is determined from calculated stress within TGO for varying thickness. Radial stresses at TGO/bond coat interface and maximum axial stresses in nanostructured zirconia coatings are found to be lower than in traditional YSZ up to a critical TGO thickness of 6 –7 μm, after which stresses in nanostructured zirconia coatings increase considerably. However, radial compressive stresses in nanostructured TBCs are lower in all TGO thickness cases and shear stresses are slightly higher with relatively more prominent difference at high oxide thickness.

Keywords: Thermal barrier coatings (TBCs); Thermally grown oxides (TGO); Interfaces; Residual stress

1. Introduction

Thermal barrier coatings (TBCs) are layer systems deposited on thermally highly loaded metallic components, as for instance in gas turbine engine blades and vanes to allow higher operating temperatures and thus to increase their efficiency and durability [1–5]. Demand for enhanced jet engine efficiencies has led to significant increase in combustion temperatures and operating pressures. These requirements have proved to be a big driving force to improve the thermal barrier coating technology, such as novel compositions, production techniques and improvement in microstructure, and physical and mechanical properties of TBCs. TBCs have typical duplex type configuration with an outer layer of compliant, porous zirconia, a film of dense aluminum oxide that grows at high temperature, a metal alloy bond coat layer from which the oxide film grows, and a thick superalloy substrate [6]. Preparation of nanostructured zirconia coating has become an active field in thermal spray industry in the last decade [7–10]. Nanostructured coatings are attractive because of their potential superior mechanical and physical properties over traditional coatings [11, 12]. The durability of thermal barrier systems is governed by a sequence of crack nucleation, propagation and coalescence events that depends on the stress state within TBC with the growth of thermally grown oxides (TGO) [6]. Thickness of TGO that is a function of thermal cycling is an important consideration to analyze the stress state in TBCs and thus plays an important role in failure studies consequent to TBC's structural integrity assessment [6,13–17]. Different studies on durability of nanostructured YSZ as compared to traditional YSZ have been reported [18–20] that describe the effect of exposure time on TGO thickness in traditional and nanostructured zirconia coatings. However, the scope of these studies is limited to the experimentally recorded data in each particular study and it still needs some quantitative comparative analysis in some methodological way, paying special attention to TGO

*Corresponding author. Tel/fax: +86 10 8231 7117.
E-mail address: guo.hongbo@buaa.edu.cn (H. Guo).

0272-8842/$36.00 © 2012 Elsevier Ltd and Techna Group S.r.l. All rights reserved.
http://dx.doi.org/10.1016/j.ceramint.2012.06.051

growth. Moreover, to identify the potential use of nanostructured YSZ in comparison with traditional zirconia coatings with TGO growth, change in stress state during oxide growth, its relation with durability and determination of critical thickness in case of nanostructured zirconia coatings are focused in this study. To cope with these arising queries in a time permissive manner, a finite element based numerical study has been carried out for traditional and nanostructured TBCs over a range of TGO thicknesses (1–12 μm). By a sequential simulation scheme with about 24 formulations for varying TGO thickness in both types of coatings, stress state at the TGO/bond coat interface, within TGO and in overall TBC system is determined, summarized graphically and compared with some novel observations.

2. Finite element model

2.1. Geometric model and FEM mesh

A circular disc specimen is considered having four layers; topcoat 200 μm, TGO 1–12 μm (varying parameter), bond coat 150 μm and substrate with thickness of 2 mm. Axisymmetric case is taken into account in the radial and through thickness directions allowing the problem to be reduced to a two-dimensional case for easy computation. A schematic illustration of the model is shown in Fig. 1. A coupled thermo-mechanical finite element solution has been employed using 2-D coupled field element PLANE223 that has eight nodes with up to four degrees of freedom per node. Due to the regular shape of the sample a mapped grid is selected for mesh construction and the geometry consists of approximately 20,000 elements. Due to the relatively small area of TGO, the regions neighboring the TGO and TGO itself are finely meshed to enhance the sensitivity to the rigorous change of stress distribution in this region.

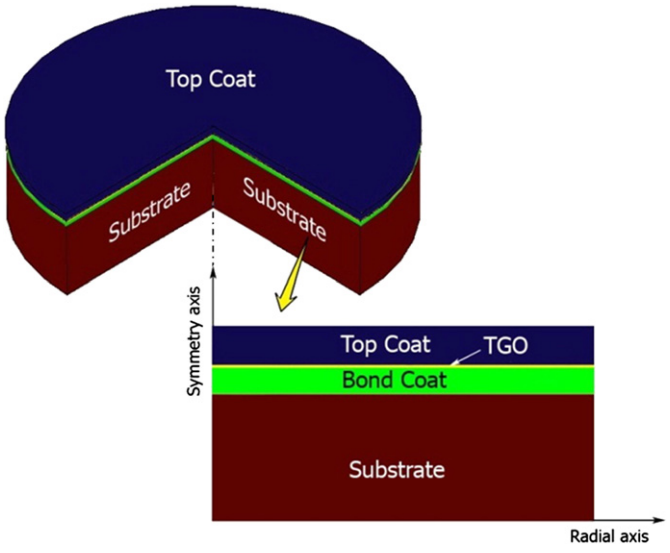

Fig. 1. Schematic illustration of coating specimen.

2.2. Materials parameters

The model has four layers: Ni-based superalloy substrate, NiCrAlY bond-coating, Al_2O_3 thermally grown oxide (TGO) and ceramic top coat. Thermal, mechanical and physical parameters of the materials used in the analysis are given in Table 1 [21,22,23].

2.3. Boundary condition

Symmetric boundary conditions are used due to the axisymmetric configuration. All layers are considered homogeneous and isotropic. The specimen is cooled from temperature 1050 °C to room temperature (25 °C) in 300 s time. Heat convection is imposed on the top and side of the sample while bottom of the specimen is assumed thermally insulated. The mechanical stress is induced during the cooling period of the thermal cycles. Phase transformation and creep mechanisms which result in stress-relieving and can effect stress state in TBCs are assumed inactive during the simulation. Peak radial tensile and compressive stresses that exist at the TGO/bondcoat interface and within TGO respectively, maximum axial stress and shear stresses within TBCs for both types of coatings are determined.

3. Results and discussion

3.1. Radial stress variation

Fig. 2 shows the variation of maximum tensile radial stress with varying TGO thickness. This stress exists at the bondcoat/TGO interface near the edge of the specimen and is important as it may propagate any pre-existing defect at the interface to increase its extent and eventually may result in TBCs failure [24]. As illustrated in Fig. 2, the interfacial stress in nanostructured TBCs remains low up to a critical TGO thickness which in this case is 6 μm. After the critical thickness of 6 μm, stress in nanostructured TBCs starts changing and keeps on increasing up to a maximum TGO thickness of 12 μm considered in this study. Higher stresses in nanostructured TBCs after a critical thickness is a novel finding that may be an important consideration for future studies on structural analysis and failure assessment of nanostructured TBCs. This finding also does not contradict to the high durability of nanostructured TBCs reported by many other researchers as nanostructured TBCs are more resistant to TGO growth [19] and it seldom exceeds the critical limit of TGO thickness found in this study. It has also been reported that the nanostructured zirconia coating has larger adhesion strength than traditional zirconia coating [22] thus having more capability to withstand high stress state. Moreover, these maximum radial stresses exist at the bondcoat/TGO interface where these two phases are more exposed to described stress state than the top coat. Thus the approximation of the thermal cycle lifetime of nanostructured TBCs needs a good estimation of stress state development

Table 1
Material performance parameters of substrate, bond coat, TGO, traditional YSZ and nano-structured YSZ.

Material	Temperature (°C)	Young's modulus (GPa)	Poisson's ratio	Thermal expansion coefficient ($\times 10^{-6}$ °C^{-1})	Thermal conductivity (W m^{-1} °C^{-1})
Ni-based alloy (substrate)	20	220	0.31	14.8	88
	200	210	0.32	15.2	73.3
	400	190	0.33	15.6	59.5
	600	170	0.33	16.2	62
	800	155	0.34	16.9	65
	1000	130	0.35	17.5	68.1
	1100	120	0.35	18	69
NiCrAlY (bond coat)	20	200	0.3	13.6	5.8
	200	190	0.3	14.2	7.5
	400	175	0.31	14.6	9.5
	600	160	0.31	15.2	12
	800	145	0.32	16.1	14.5
	1000	120	0.33	17.2	16.2
	1100	110	0.33	17.6	17
Al_2O_3 (thermally grown oxide)	20	400	0.23	8	10
	200	390	0.23	8.2	7.794
	400	380	0.24	8.4	6.029
	600	370	0.24	8.7	5.074
	800	355	0.25	9	4.412
	1000	325	0.25	9.3	4.412
	1100	320	0.25	9.6	4
Traditional YSZ (top coat)	20	48	0.1	9	1.956
	200	47	0.1	9.2	1.834
	400	44	0.1	9.6	1.736
	600	40	0.11	10.1	1.627
	800	34	0.11	10.8	1.634
	1000	26	0.12	11.7	1.681
	1100	22	0.12	12.2	1.7
Nano-structured YSZ (top coat)	100	60	0.23	10.7	1.11
	300	58	0.23	11.1	1.06
	500	44	0.24	11.2	0.02
	700	38	0.24	11.3	1.0
	900	36	0.25	11.4	0.99
	1000	34	0.25	11.5	1.01
	1100	32	0.25	11.6	1.12

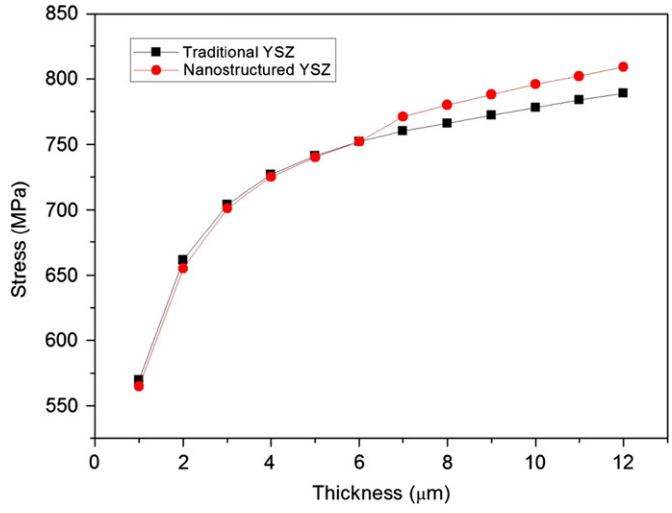

Fig. 2. Radial tensile stress in traditional and nanostructured YSZ coatings as a function of TGO thickness.

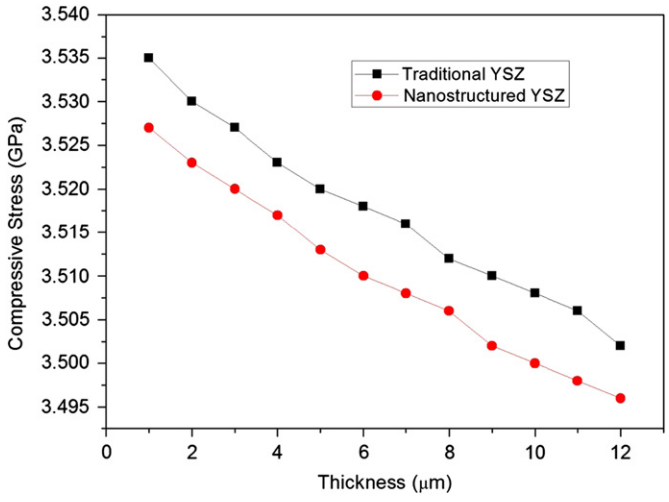

Fig. 3. Radial compressive stress in traditional and nanostructured YSZ coatings as a function of TGO thickness.

combined with TGO growth during the course of thermal exposure. Fig. 3 shows residual compression stresses for considered TGO thickness range for both traditional and nanostructured TBCs. These stresses are developed due to the difference in thermal expansion between TGO layer and bond coat [6]. Fig. 3 shows that compressive stresses for both TBCs drop proportionally with increase in TGO thickness. However, the compressive stresses in nanostructure TBC at all TGO thicknesses are slightly lower than in traditional TBCs. The durability of the TBC is controlled by the energy density in the TGO and is analyzed by calculating the total elastic strain energy per unit area. It is given as follows [25]:

$$G_o = \frac{(1-v_{ox})h_{ox}\sigma_{ox}^2}{E_{ox}} \quad (1)$$

Where G_o is the elastic strain energy, v_{ox} is poisson's ratio of TGO, h_{ox} is the TGO thickness, σ_{ox} is stress within TGO and E_{ox} is the elastic modulus of TGO. Fracture of TGO is possible when $G_o > \Gamma_o$, where Γ_o is the fracture toughness of the interface [25]. Fig. 4 shows the elastic strain energy G_o for the both coatings systems with varying oxide

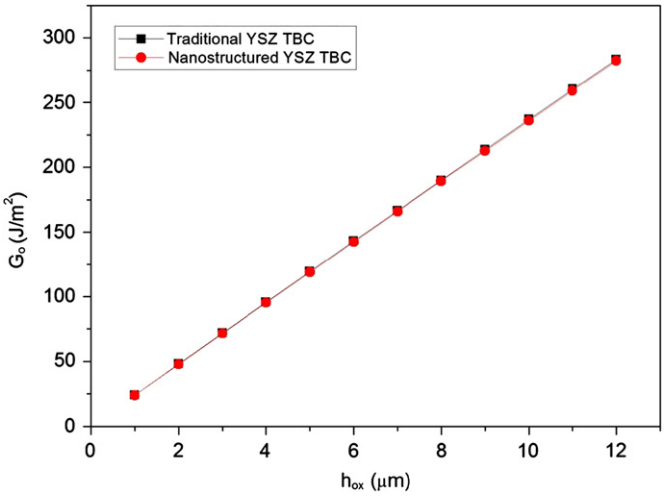

Fig. 4. Elastic strain energy within TGO for traditional and nanostructured YSZ coatings.

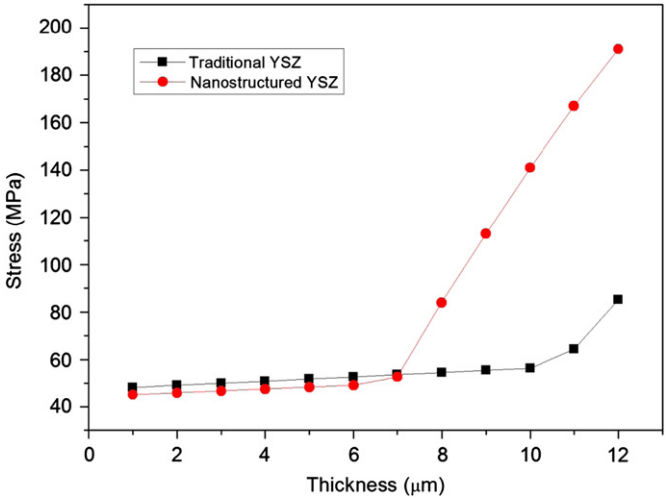

Fig. 6. Axial tensile stresses in traditional and nanostructured YSZ coatings as a function of TGO thickness.

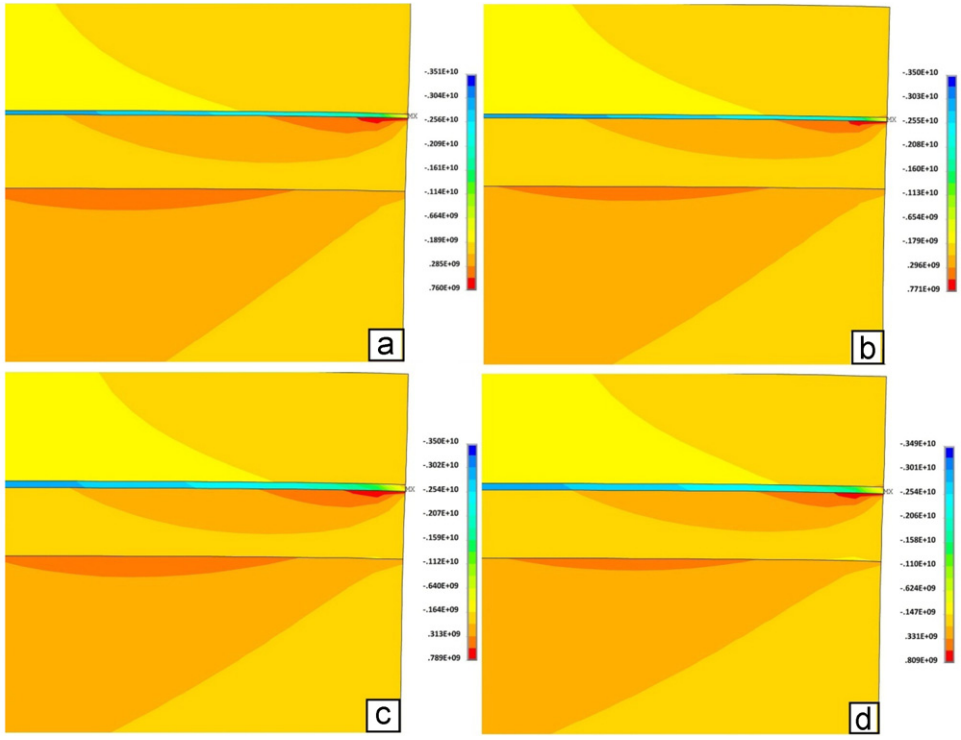

Fig. 5. Contour plot of radial stress (σ_{xx}) distribution in (left) traditional and (right) nanostructured YSZ coatings at 7 μm (a, b) and 12 μm (c, d) TGO thickness.

thickness computed from the numerically calculated stress value in TGO from finite element (FE) analysis. Fig. 4 shows that the elastic strain energy increases linearly with increase in TGO thickness and is the same for traditional and nanostructured coating systems as both lines are superimposed on each other. It implies that if Γ_o for TGO of both coatings are assumed same, both coatings have equally high risk of spall within TGO due to the stress state arising from TGO growth. The stress state in radial direction for two TGO thicknesses 7 μm and 12 μm for both TBCs is shown in Fig. 5. It can be noted from Fig. 5 that the stress distribution in both TBCs is almost in a similar fashion. The difference only lies in peak stress values in both tension and compression which have been explained earlier in Figs. 2 and 3 .

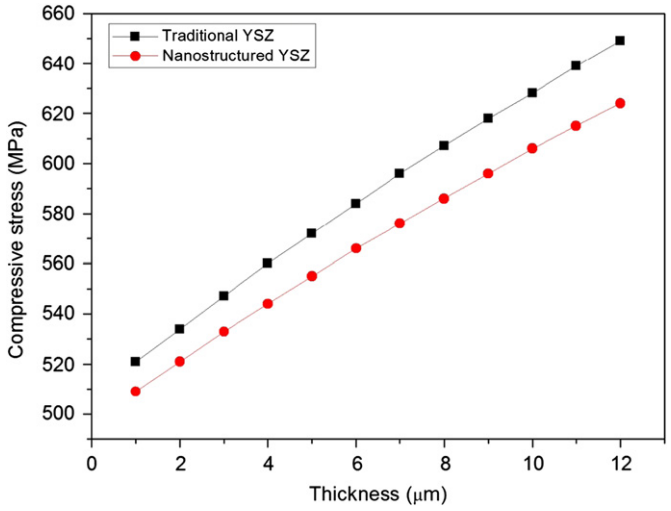

Fig. 7. Axial compressive stresses in traditional and nanostructured YSZ coatings as a function of TGO thickness.

3.2. Axial stress variation

Comparison of peak axial stress in nanostructured and traditional TBCs is presented in Fig. 6 where stress variation with increasing TGO thickness is explained. Similar to radial stresses, axial stresses in nanostructured TBCs are lower than in traditional TBC up to a critical TGO thickness which in the present case is 7 μm. Difference in the stress state is almost constant up to 6 μm which was found to be a critical TGO thickness value in case of radial stresses. Beyond 7 μm TGO growth, axial stresses in nanostructured TBC increase drastically and expose nanostructured zirconia coating to unstable bending more vigorously than the traditional zirconia coating due to the high normal stress in the former. Variation in axial compressive stresses for both coatings has been presented in Fig. 7, which shows that compressive stresses in nanostructured coating are lower than those in traditional coatings in all TGO thickness cases. The stress state in normal direction is further elaborated with the contour plot of axial stress for 7 μm and 12 μm TGO thickness cases presented in Fig. 8. As shown in Fig. 8, maximum axial stress in all cases, except in 7 μm TGO-traditional coating case, exists at the ceramic coat/TGO interface and as explained by Hsueh and Fuller [26], these residual

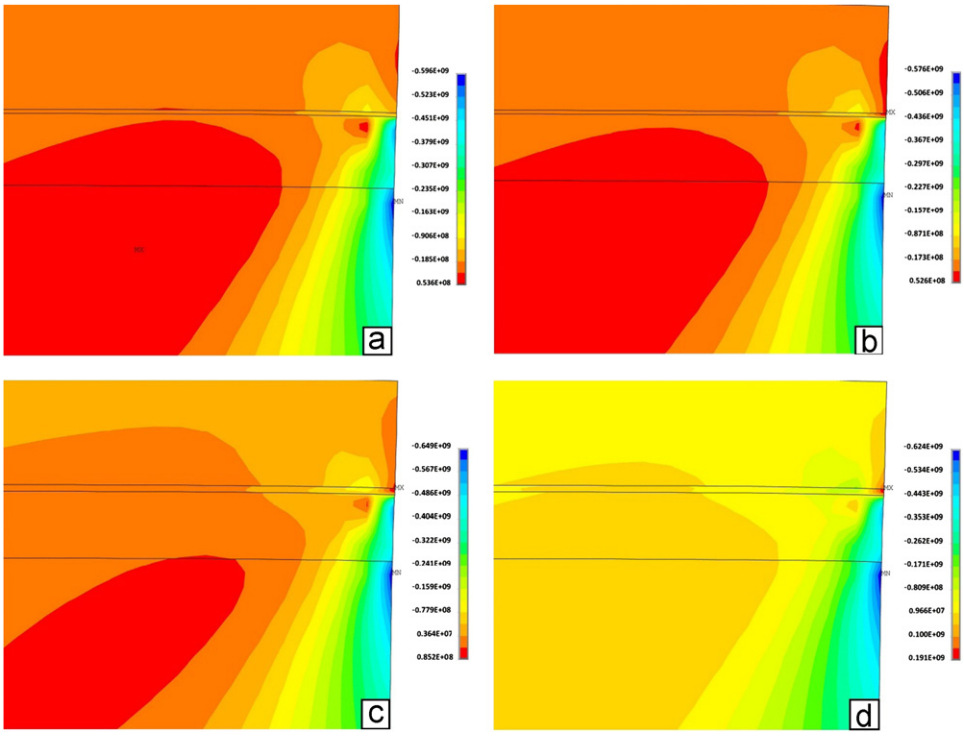

Fig. 8. Contour plot of axial stress (σ_{yy}) distribution in (left) traditional and (right) nanostructured YSZ coatings at 7 μm (a, b) and 12 μm (c, d) TGO thickness.

stresses normal to the interface between the ceramic top coat and the TGO may result in the cracking and spallation of TBC. This effect is more likely to occur in nanostructured coating with high TGO thickness due to the high stress development as anticipated and explained before in Fig. 6. Moreover, maximum axial compressive stress may also be important as in all cases it exists near the bondcoat/substrate interface and it will be more significant if some oxide network is also present at bond coat/substrate. The oxides formed here are believed to be of spinel type [27,28], giving the interface poor mechanical properties and thus any stress state near bond coat/substrate may also be an important consideration.

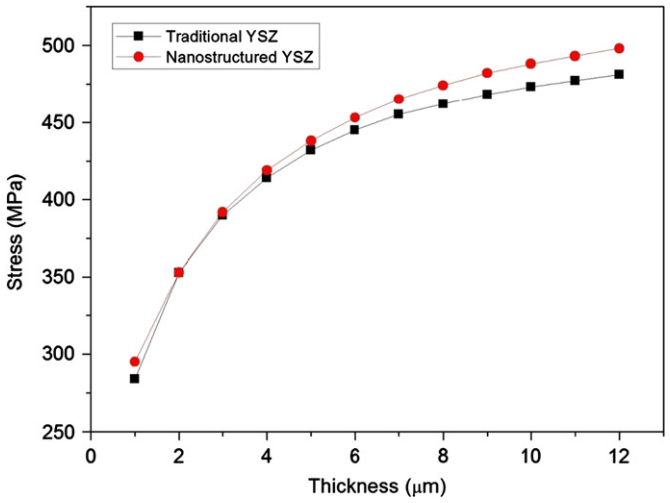

Fig. 9. Shear stresses in traditional and nanostructured YSZ coatings as a function of TGO thickness.

3.3. Shear stress variation

Fig. 9 presents the variation in shear stress in traditional and nanostructured coatings for varying TGO thickness. The figure shows that shear stress increases with the increase in TGO thickness in both coating systems. However, the shear stress value in nanostructured coating is higher than in traditional coating and the difference increases proportionally with the increase of TGO thickness. The shear stress pattern in both coating systems for 7 μm and 12 μm TGO thickness cases is presented in Fig. 10. As shown in Fig. 10 the shear stress distribution in all cases is almost same with the difference of peak stress values. Moreover, the stress concentration is observed at the metallic bond coat/TGO interface and may play an important role in decohesion of the layers leading to buckling instability and failure of TBCs.

These abrupt changes in stresses in radial and axial directions are likely to be due to differential thermo-physical properties of nanostructured topcoat and TGO. Nanostructured YSZ has high thermal expansion and low thermal conductivity as compared to TGO and traditional YSZ. Since TGO lies beneath topcoat in the TBC system, its effect with increasing its volume to some critical value likely results in a drastic change in the stress state.

Based on the results presented, it can be concluded that to get the potential advantages of nanostructured zirconia coating, TGO growth as a function of thermal cycles must

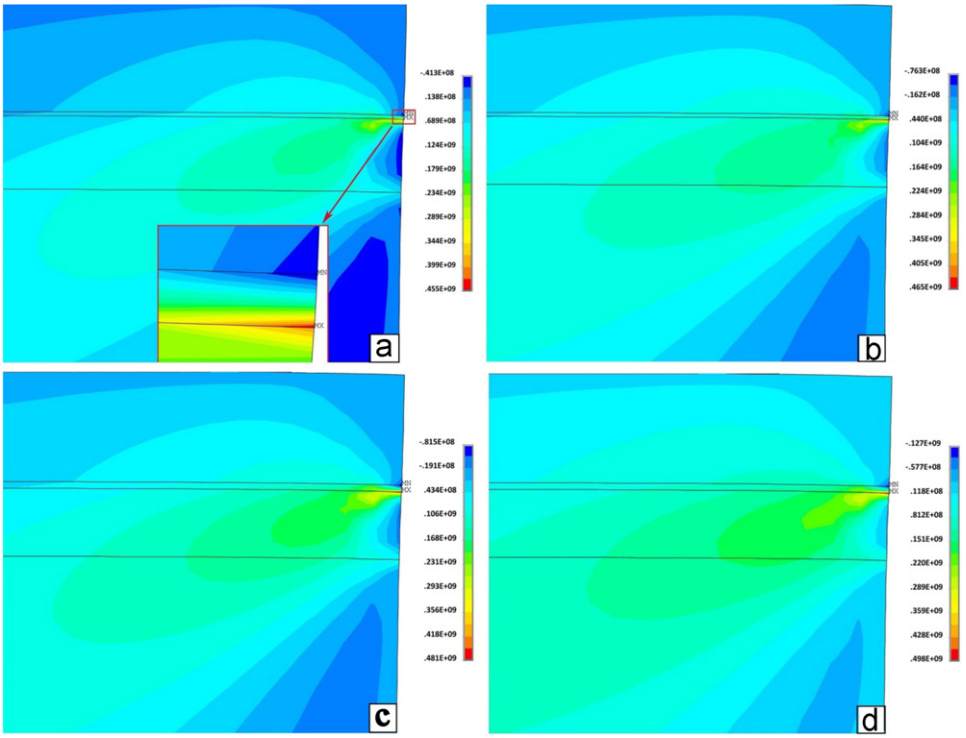

Fig. 10. Contour plot of shear stress (σ_{xy}) distribution in (left) traditional and (right) nanostructured YSZ coatings at 7 μm (a, b) and 12 μm (c, d) TGO thickness.

properly be investigated when estimating the lifetime of the coatings. Although nanostructured zirconia coatings are believed to be more resistant to TGO growth and are considered stronger than those of traditional zirconia, however there is still need for better structural integrity assessment based on stress distribution and its variation with TGO growth, for which the present study may be helpful especially to determine the lifetime of TBCs based on TGO growth.

4. Conclusion

In the present study stress response of traditional and nanostructured YSZ coatings has been analyzed with varying TGO thickness. It has been found that tensile radial and axial stresses in nanostructured YSZ coating are lower than in traditional coatings up to about 6–7 μm TGO thickness with almost uniform difference. Beyond that these stresses in nanostructured coating become higher and the difference keeps on increasing up to a maximum thickness of 12 μm considered in this study. However, radial compressive stresses are lower in nanostructured coatings than in traditional coatings at all TGO thicknesses with almost a constant difference. Elastic strain energy (G_o) associated with stress state within TGO is calculated for both coatings systems as a function of TGO thickness. It is found that the trend of increase in G_o for TGO of both coating systems is almost same, connoting its same effect on both coating systems.

References

[1] K. Kokini, Y.R. Takeuchi, B.D. Choules, Thermal crack initiation mechanisms on the surface of functionally graded ceramic thermal barrier coatings, Ceramics International 22 (1996) 397–401.

[2] S. Guo, Y. Kagawa, Young's moduli of zirconia top-coat and thermally grown oxide in a plasma-sprayed thermal barrier coating system, Scripta Materialia 50 (2004) 1401–1406.

[3] J. Wu, Hongbo Guo, M. Abbas, S. Gong, Evaluation of plasma sprayed YSZ thermal barrier coatings with the CMAS deposits infiltration using impedance spectroscopy, Progress in Natural Science: Materials. International 22 (1) (2012) 40–47.

[4] N.P. Padture, M. Gell, E.H. Jordan, Thermal barrier coatings for gas-turbine engine applications, Science 296 (2002) 280.

[5] R. Vaßen, M.O. Jarligo, T. Steinke, D.E. Mack, D. Stöver, Overview on advanced thermal barrier coatings, Surface and Coatings Technology 205 (2010) 938–942.

[6] A.G. Evans, D.R. Mumm, J.W. Hutchinson, G.H. Meier, F.S. Petitt, Mechanisms controlling the durability of thermal barrier coatings, Progress In Materials Science 46 (2001) 505–553.

[7] M. Gell, Application opportunities for nanostructured materials and coatings, Materials Science and Engineering A204 (1995) 246–251.

[8] R.S. Lima, A. Kucuk, C.C. Berndt, Evaluation of microhardness and elastic modulus of thermally sprayed nanostructured zirconia coatings, Surface and Coatings Technology 135 (2001) 166–172.

[9] H. Chen, Y. Zeng, C.X. Ding, Microstructural characterization of plasma-sprayed nanostructured zirconia powders and coatings, Journal of the European Ceramic Society 23 (2003) 491–497.

[10] Y. Zeng, S.W. Lee, L. Gao, C.X. Ding, Atmospheric plasma sprayed coatings of nanostructured zirconia, Journal Of The European Ceramic Society 22 (2002) 347–351.

[11] B.H. Kear, P.R. Strutt, Chemical processing and applications for. nanostructured materials, Nanostructured Materials 6 (1–4) (1995) 227–236.

[12] Bo Liang, H. Liao, C. Ding, C. Coddet, Nanostructured zirconia–30 vol.% alumina composite coatings deposited by atmospheric plasma spraying, Thin Solid Films 484 (2005) 225–231.

[13] D.R. Clarke e, W. Pompe, Critical radius for interface separation of a compressively stressed film from a rough surface, Acta Materialia 47 (6) (1999) 1749–1756.

[14] K.W. Schlichting, N.P. Padture, E.H. Jordan, M. Gell. Failure modes in plasma-sprayed thermal barrier coatings, Materials Science and Engineering., A, 342, 120-130 (2003).

[15] K. Vaidyanathan, E.H. Jordan, M. Gell, Surface geometry and strain energy effects in the failure of (Ni/Pt)/Al EB-PVD thermal barrier coating, Acta Materialia 52 (2004) 1107–1115.

[16] A.G. Evans, M.Y. He, J.W. Hutchinson, Mechanics-based scaling laws for the durability of thermal barrier coatings, Progress in Materials Science 46 (2001) 249.

[17] G.M. Kim1, N.M. Yanar, E.N. Hewitt, F.S. Pettit, G.H. Meier, The effect of the type of thermal exposure on the durability of thermal barrier coatings, Scripta Materialia 46 (2002) 489–495.

[18] L. Chun-bo, Z. Zhi-min, J.X. liang, L. Min, Z. Zhao-hui, Comparison of thermal shock behaviors between plasma-sprayed nanostructured and conventional zirconia thermal barrier coatings, Transactions of the Nonferrous Metals Society of China 19 (2009) 99–107.

[19] Kaka Ma, J.M. Schoenung, Isothermal oxidation behavior of cryomilled NiCrAlY bond coat: homogeneity and growth rate of TGO, Surface and Coatings Technology 205 (2011) 5178–5185.

[20] A. Keyvani, M. Saremi, M.H. Sohi, An investigation on oxidation, hot corrosion and mechanical properties of plasma-sprayed conventional and nanostructured YSZ coatings, Surface and Coatings Technology 206 (2011) 208–216.

[21] A. Liu, Y. Wei, Finite element analysis of anti-spallation thermal barrier coatings, Surface and Coatings Technology 165 (2003) 154–162.

[22] H. Chen, X. Zhou, C. Ding, Investigation of the thermomechanical properties of a plasma-sprayed nanostructured zirconia coating, Journal of the European Ceramic Society 23 (2003) 1449–1455.

[23] C. Zhou, Na Wang, H. Xu, Comparison of thermal cycling behavior of plasma-sprayed nanostructured and traditional thermal barrier coatings, Materials Science and Engineering A 452–453 (2007) 569–574.

[24] H. Bhatnagar, S. Ghosh, M.E. Walter, Parametric studies of failure mechanisms in elastic EB-PVD thermal barrier coatings using FEM, International Journal of Solids and Structures 43 (2006) 4384–4406.

[25] P.K. Wright, A.G. Evans, Mechanisms governing the performance of thermal barrier coatings, Current Opinion in Solid State and Materials Science 4 (1999) 255–265.

[26] C.H. Hsueh, E.R. Fuller Jr, Analytical modeling of oxide thickness effects on residual stresses in thermal barrier coatings, Scripta Materialia 42 (2000) 781–787.

[27] E.A.G. Shillington, D.R. Clarke, Spalling failure of a thermal barrier coating associated with aluminum depletion in the bond-coat, Acta Materialia 47 (1999) 1297–1305.

[28] J.A. Haynes, M.K. Ferber, W.D. Porter, E.D. Rigney, Mechanical properties and fracture behavior of interfacial alumina scales on plasma-sprayed thermal barrier coatings, Materials at High Temperatures 16 (1999) 49–69.